

COVER PAGE

Document downloaded by @DAEL

Sun Nov 29 09:34:09 2026
For personal use

When automatic English translation is provided, only the original document is authentic.
The EAA cannot be held responsible of any translation error

Bibliographical reference

Thermal-Mechanical Wave Propagation in Inviscid Non-Uniform Flow Confined by Heating Pipeline and Implications for Transit-Time Flow Meter, Yong Chen, Yiyong Huang and Xiaoqian Chen, Acta Acustica **vol. 99** (Number 4), 2013, pp. 503-513

DOI
https://doi.org/10.3813/AAA.918630

ACTA ACUSTICA UNITED WITH ACUSTICA
Vol. 99 (2013) 503 – 513

Scientific Papers
DOI 10.3813/AAA.918630

Thermal-Mechanical Wave Propagation in Inviscid Non-Uniform Flow Confined by Heating Pipeline and Implications for Transit-Time Flow Meter

Yong Chen, Yiyong Huang, Xiaoqian Chen
Institute of Space Technology, College of Aerospace Science and Engineering,
National University of Defense Technology, 410073, Changsha, China.
literature.chen@gmail.com, yiyong_h@sina.com chenxiaoqian@nudt.edu.cn

Summary
Thermal-mechanical wave propagation (phase velocity, distributions of acoustic pressure and temperature) in inviscid non-uniform flow confined by heating circular pipeline is mathematically formulated from conservations of continuity, momentum, and energy. A novel solution in the form of zeroth-order Bessel series, which are complete and orthogonal in Lebesgue Space, is proposed to regulate the high-order differential equations to algebraic linear equations. As a result, the problem is solved by non-trivial solution of homogeneous linear equations. Based on the proposed method, phase velocity, and pressure and temperature distribution in the presence of axial temperature gradient are comprehensively analyzed in both laminar and turbulent flow. Furthermore, measurement performance of ultrasonic transit-time flow meter is investigated in both laminar and turbulent flow with variations of ultrasound frequency, pipeline radii, and axial temperature gradient. It is shown that temperature gradient imposes outstanding influence on phase velocity and measurement performance. Another point is that decreasing the cylinder radius and ultrasound frequency are effective ways to diminish the influence of temperature gradient for laminar flow, however, in turbulent flow, measurement accuracy with lower frequency is worse than higher frequency.

PACS no. 43.20.Bi, 43.20.Mv, 43.28.Py, 43.35.Ud, 43.45.Zc

1. Introduction

In many practical situations, e.g. district-heating applications, temperature gradient exists in the fluid [1, 2]. Thus, wave propagation in fluid is affected as it propagates along the heating pipeline filled with moving fluid. This behaviour is dependent on, among other parameters, the flow regime and the pipelines' geometrical and physical characteristics [3]. A very important issue to address is whether such temperature gradient affects the accuracy of ultrasonic flow meter and to what extent. As a result, prediction of thermal-mechanical wave propagation in non-uniform moving flow confined by heating pipeline helps to select appropriate operational parameters, which in turn optimizes the system performance. For measurement of low liquid flow rate, M. Law [4] introduced an ultrasonic flow meter based on the interaction of ultrasound and fluid temperature generated by electrical heaters.

In the case of dynamics of wave propagation in non-moving flow, Pridmore [5] established the wave equation in non-uniform flow for two-dimensional rectangular duct and Mungur [6] for the circular duct. Following the pioneering work, investigators dealt with the problem using various numerical methods, such as Runge-Kutta method [6, 7], Galerkin based method [8, 9, 10] , iterative method [11, 12], wave envelope analysis [13] and discretization method [14, 15, 16, 17, 18, 19]. On the other hand, analytical and semi-analytical methods were shown in the literature, such as weighted residual theory [20, 21, 22, 23], combination of residual and Sturm-Liouville theory [24], Kummer differential equation theory [25, 26, 27, 28]. To analyze the performance of ultrasonic flow meter, Lechner [29] and Willatzen [30] introduced an approximation based on local-plane-wave (LPW) acoustics propagation on the assumption that wave propagates parallel along the flow direction, a condition only holds in the case of fundamental mode wave propagation. Willatzen [31] later compared the difference between LPW and wave equation of Mungur using a quasi-analytical frobenius power series expansion technique [32], based on the separability of the eigenfunction [31, 33]. Perturbation method [34, 35] was used by Willatzen [36] and Wendoloskia [37] to analyze the influence of low Mach non-uniform flow on wave

Received 30 May 2012,
accepted 3 April 2013.

© S. Hirzel Verlag · EAA

propagation. Using Lagrangian specification, Treyssede [38, 39] expressed the wave equation based on Galbrun's theory and solved the problem by finite element discretization method. Although numerical method can give approximation solutions, an analytical description can provide more physical insight into global behavior of wave propagation than numerical discretization solution.

For wave propagation confined by heating pipeline, many researchers have made wonderful contributions and a good summarization can be found in [2]. Willatzen [1, 2] gave an analysis of wave propagation in the presence of axial temperature gradient and showed the influence of temperature gradient on transit-time flow measurement for laminar flow profile. However, in Willatzen's work, the dynamics of temperature is not considered and wave propagation in turbulent flow isn't addressed.

In the present work, based on the excellent work of Willatzen, a detailed mathematical formulation of thermal-mechanical wave propagation in inviscid non-uniform flow confined by heating pipeline is addressed, showing to be two second-order differential equations. Then a novel solution in the form of Bessel functions, which are orthogonal and complete in Lebesgue Space [40, 41, 42], is proposed. Such method has the advantage of transforming the two second-order differential equations to algebraic equations which can be solved by existence condition of non-trivial solution for linear algebraic equations. Based on the established method, phase velocity, acoustic pressure and temperature distribution in the circular cross section are accounted for both laminar and turbulent flow. Finally, parametric analysis of transit-time flow meter performance is investigated for laminar and turbulent flow profile where different ultrasound frequency, pipeline radii and temperature gradients are considered.

The layout of the paper is as follows. In section 2, a general description of thermal-mechanical wave propagation in non-uniform flow is mathematically formulated, and a novel solution in the form of Bessel series is proposed to convert the high-order differential equations to algebraic equations. In the end, a general calculation procedure for the algebraic equations is given. Section 3 gives a comprehensive parametric analysis of thermal-mechanical wave propagation in laminar and turbulent flow confined by heating pipeline, and measurement performance of ultrasonic transit-time flow meter is discussed. Finally conclusions are drawn in section 4.

2. Wave propagation in inviscid thermal fluid flow

2.1. Mathematical formulation of nonisentropic flow acoustics

Let us consider thermal-mechanical wave propagation in inviscid homogeneous fluid confined by rigid cylindrical pipeline as shown in Figure 1.

The basic equations governing the dynamics of velocity, pressure, and energy in inviscid fluid are conservation of

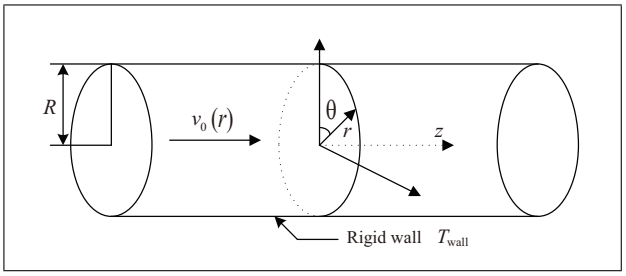

Figure 1. Cylindrical waveguide with coordinate system. R is the radius of the pipeline with rigid wall with temperature T_{wall}, and $v_0(r)$ is the velocity profile of the axial mean flow.

mass,

$$\frac{\partial \rho}{\partial t} + \nabla \cdot (\rho \boldsymbol{v}) = 0, \tag{1}$$

conservation of momentum,

$$\frac{\partial \boldsymbol{v}}{\partial t} + (\boldsymbol{v} \cdot \nabla)\boldsymbol{v} = \frac{\nabla p}{\rho}, \tag{2}$$

conservation of energy [43, 44],

$$\rho T\left(\frac{\partial s}{\partial t} + (\boldsymbol{v} \cdot \nabla)s\right) = \kappa \nabla^2 T, \tag{3}$$

where p, $\boldsymbol{v} = [v_1, v_2, v_3]$, T, and s denote pressure, velocity, temperature, and entropy. ρ and κ are the density and thermal conductivity.

From the theory of thermodynamics [45], ρ and s can be expressed as functions of p and p,

$$\begin{aligned} \frac{\partial s}{\partial t} &= \frac{c_p}{T}\frac{\partial T}{\partial t} - \frac{\beta}{\rho}\frac{\partial p}{\partial t}, \\ \nabla s &= \frac{c_p}{T}\nabla T - \frac{\beta}{\rho}\nabla p, \end{aligned} \tag{4}$$

where β is the coefficient of volume expansion and c_p is the specific heat capacity at constant pressure. Substituting equation (4) into equation (3) gives [46]

$$\begin{aligned} &\frac{\partial T}{\partial t} + (\boldsymbol{v} \cdot \nabla)T = \\ &\quad \frac{\kappa}{\rho c_p}\nabla^2 T + \frac{\beta T}{\rho c_p}\left(\frac{\partial p}{\partial t} + (\boldsymbol{v} \cdot \nabla)p\right), \end{aligned} \tag{5}$$

as shown by Fetter [44], for liquid $\beta = 0$. Then equation (5) is rewritten by

$$\frac{\partial T}{\partial t} + (\boldsymbol{v} \cdot \nabla)T = \frac{\kappa}{\rho c_p}\nabla^2 T. \tag{6}$$

When fluid experiences a small-amplitude disturbance, its ambient physical variables (denoted by a subscript zero) are modified to

$$\begin{aligned} &\boldsymbol{v} = \boldsymbol{v}_0 + \boldsymbol{v}', \quad p = p_0 + p', \\ &\rho = \rho_0 + \rho', \quad T = T_0 + T', \quad \rho_0 = \text{constant}. \end{aligned} \tag{7}$$

Substituting equation (7) into equations (1), (2), and (6) gives the governing equations of thermal-mechanical wave propagation

$$\frac{\partial \rho'}{\partial t} + \big(\boldsymbol{v}_0 \cdot \nabla\big)\rho' + \rho_0 \nabla \cdot \boldsymbol{v}' = 0,$$

$$\begin{aligned}
&\frac{\partial \boldsymbol{v}'}{\partial t} + \big(\boldsymbol{v}' \cdot \nabla\big)\boldsymbol{v}_0 + \big(\boldsymbol{v}_0 \cdot \nabla\big)\boldsymbol{v}' = \frac{\nabla p'}{\rho_0} + \frac{\nabla p_0 \rho'}{\rho_0^2},\\
&\frac{\partial T'}{\partial t} + \big(\boldsymbol{v}' \cdot \nabla\big)T_0 + \big(\boldsymbol{v}_0 \cdot \nabla\big)T' = \frac{\kappa}{\rho_0 c_p}\nabla^2 T', \qquad (8)
\end{aligned}$$

and the steady flow is governed by

$$\begin{aligned}
&\nabla \cdot \big(\rho_0 \boldsymbol{v}_0\big) = 0, \qquad \big(\boldsymbol{v}_0 \cdot \nabla\big)\boldsymbol{v}_0 = -\frac{\nabla p_0}{\rho_0},\\
&\big(\boldsymbol{v}_0 \cdot \nabla\big)T_0 = \frac{\kappa}{\rho_0 c_p}\nabla^2 T_0, \qquad T_0\big|_{r=R} = T_{\text{wall}}, \qquad (9)
\end{aligned}$$

where T_{wall} is the temperature of the wall as shown in Figure 1. Assume the flow is taken to be axially symmetric with flow profile $\boldsymbol{v} = [0, 0, v_0(r)]$ as shown in Figure 1, there is

$$\big(\boldsymbol{v}_0 \cdot \nabla\big)\boldsymbol{v}_0 = -\frac{\nabla p_0}{\rho_0} = 0 \quad \Rightarrow \quad \nabla p_0 = 0. \qquad (10)$$

Substituting equation (10) into the second equation of (8) gives

$$\begin{aligned}
&\frac{\partial \rho'}{\partial t} + \big(\boldsymbol{v}_0 \cdot \nabla\big)\rho' + \rho_0 \nabla \cdot \boldsymbol{v}' = 0,\\
&\frac{\partial \boldsymbol{v}'}{\partial t} + \big(\boldsymbol{v}' \cdot \nabla\big)\boldsymbol{v}_0 + \big(\boldsymbol{v}_0 \cdot \nabla\big)\boldsymbol{v}' = -\frac{\nabla p'}{\rho_0}, \qquad (11)\\
&\frac{\partial T'}{\partial t} + \big(\boldsymbol{v}' \cdot \nabla\big)T_0 + \big(\boldsymbol{v}_0 \cdot \nabla\big)T' = \frac{\kappa}{\rho_0 c_p}\nabla^2 T'.
\end{aligned}$$

From [45] and $\beta = 0$, the equation of liquid state can be written as

$$\rho' = \frac{1}{c_0^2(T_0)} p', \qquad (12)$$

where $c_0(T_0)$ is the adiabatic velocity of sound and a function of steady temperature T_0. Substituting equation (12) into the first equation of (11) shows

$$\begin{aligned}
&\frac{\partial p'}{\partial t} + \big(\boldsymbol{v}_0 \cdot \nabla\big)p' + \rho_0 c_0^2(T_0)\nabla \cdot \boldsymbol{v}' = 0,\\
&\frac{\partial \boldsymbol{v}'}{\partial t} + \big(\boldsymbol{v}' \cdot \nabla\big)\boldsymbol{v}_0 + \big(\boldsymbol{v}_0 \cdot \nabla\big)\boldsymbol{v}' = -\frac{\nabla p'}{\rho_0}, \qquad (13)\\
&\frac{\partial T'}{\partial t} + \big(\boldsymbol{v}' \cdot \nabla\big)T_0 + \big(\boldsymbol{v}_0 \cdot \nabla\big)T' = \frac{\kappa}{\rho_0 c_p}\nabla^2 T'.
\end{aligned}$$

For monochromatic acoustic ($\exp(\mathrm{j}\omega t)$) propagation, with $\omega\ (= 2\pi f)$ being the angular frequency, equation (13) becomes

$$\begin{aligned}
&\mathrm{j}\omega p' + \big(\boldsymbol{v}_0 \cdot \nabla\big)p' + \rho_0 c_0^2(T_0)\nabla \cdot \boldsymbol{v}' = 0,\\
&\mathrm{j}\omega \boldsymbol{v}' + \big(\boldsymbol{v}' \cdot \nabla\big)\boldsymbol{v}_0 + \big(\boldsymbol{v}_0 \cdot \nabla\big)\boldsymbol{v}' = -\frac{\nabla p'}{\rho_0}, \qquad (14)\\
&\mathrm{j}\omega T' + \big(\boldsymbol{v}' \cdot \nabla\big)T_0 + \big(\boldsymbol{v}_0 \cdot \nabla\big)T' = \frac{\kappa}{\rho_0 c_p}\nabla^2 T'.
\end{aligned}$$

Consider wave propagation in the axis-symmetric case where there are no tangential variations and the unsteady part of the velocity of fluid particles can be expressed as $\boldsymbol{v}' = [v_r', v_z']$. The velocity of fluid particles can be obtained by the second equation of (14)

$$\begin{aligned}
v_r' &= \frac{\mathrm{j}}{\rho_0\big(\omega - k_z v_0(r)\big)}\frac{\partial p'}{\partial r},\\
v_z' &= \frac{k_z}{\rho_0\big(\omega - k_z v_0(r)\big)}p' \qquad (15)\\
&\quad - \frac{1}{\rho_0\big(\omega - k_z v_0(r)\big)^2}\frac{\mathrm{d}p'}{\mathrm{d}r}.
\end{aligned}$$

In axial symmetric cylindrical coordinate as shown in Figure 1, the pressure and temperature in equation (14) can be expressed by

$$\begin{aligned}
p'(r, z; t) &= \varphi_p(r)\exp\big(\mathrm{j}(\omega t - k_z z)\big),\\
T'(r, z; t) &= \varphi_T(r)\exp\big(\mathrm{j}(\omega t - k_z z)\big), \qquad (16)
\end{aligned}$$

where $\varphi_p(r)$ and $\varphi_T(r)$ are continuous differentiable functions in the range $r \in [0, R]$ and satisfy

$$\begin{aligned}
&\int_0^R \big|\varphi_p(r)\big|^4 \mathrm{d}r < +\infty,\\
&\int_0^R \big|\varphi_T(r)\big|^4 \mathrm{d}r < +\infty. \qquad (17)
\end{aligned}$$

Substituting equation (16) into (14) and (15) yields

$$\begin{aligned}
&\frac{\mathrm{d}^2\varphi_p}{\mathrm{d}r^2} + \left(\frac{1}{r} + \frac{2k_z}{\omega - k_z v_0(r)}\frac{\mathrm{d}v_0(r)}{\mathrm{d}r}\right)\frac{\mathrm{d}\varphi_p}{\mathrm{d}r}\\
&\qquad + \left(\frac{\big(\omega - k_z v_0(r)\big)^2}{c_0^2(T_0)}\right)\varphi_p = 0,\\
&\frac{\kappa}{\rho_0 c_p}\left(\frac{1}{r}\frac{\mathrm{d}}{\mathrm{d}r}\left(r\frac{\mathrm{d}\varphi_T}{\mathrm{d}r}\right) - k_z^2\varphi_T\right) - \mathrm{j}\big(\omega - k_z v_0(r)\big)\varphi_T\\
&= \frac{\mathrm{j}}{\rho_0\big(\omega - k_z v_0(r)\big)} \qquad (18)\\
&\left(\frac{\partial T_0}{\partial r} + \frac{\mathrm{j}}{\rho_0\big(\omega - k_z v_0(r)\big)}\frac{\partial T_0}{\partial z}\frac{\mathrm{d}v_0(r)}{\mathrm{d}r}\right)\frac{\mathrm{d}\varphi_p}{\mathrm{d}r}\\
&+ \left(\frac{k_z}{\rho_0\big(\omega - k_z v_0(r)\big)}\frac{\partial T_0}{\partial r} - \frac{\partial T_0}{\rho_0 c_0^2(T_0)\partial z}v_0(r)\right)\varphi_p.
\end{aligned}$$

In the case of ultrasonic flow-meter applications in, e.g., water-transport systems or district-heating systems, the assumption [1, 31, 47] that flow velocity $v_0(r)$ is smaller than the phase speed ω/k_z is made with $k_z v_0(r)/\omega \ll 1$, then using Taylor expansion and omitting higher order terms, equation (18) can be rewritten as

$$\begin{aligned}
&\frac{\mathrm{d}^2\varphi_p}{\mathrm{d}r^2} + \left(\frac{1}{r} + \frac{2k_z}{\omega}\left(\frac{k_z v_0(r)}{\omega}\right)\frac{\mathrm{d}v_0(r)}{\mathrm{d}r}\right)\frac{\mathrm{d}\varphi_p(r)}{\mathrm{d}r}\\
&\qquad + \left(\frac{\omega^2 - 2k_z\omega v_0(r)}{c^2(T_0)} - k_z^2\right)\varphi_p(r) = 0,
\end{aligned}$$

$$\kappa\frac{1}{r}\frac{\mathrm{d}}{\mathrm{d}r}\left(r\frac{\mathrm{d}\varphi_T(r)}{\mathrm{d}r}\right)+\left(\mathrm{j}\left(k_z v_0(r)-\omega\right)-\kappa k_z\right)\varphi_T(r)$$
$$=-\frac{\mathrm{j}}{\rho_0\omega}\left(1+\frac{k_z v_0(r)}{\omega}\right)\frac{\partial T_0}{\partial r}\frac{\mathrm{d}\varphi_p(r)}{\mathrm{d}r}$$
$$-\frac{\partial T_0}{\partial z}\left(\frac{k_z}{\rho_0\omega}\left(1+\frac{k_z v_0(r)}{\omega}\right)\varphi_p(r)\right.$$
$$\left.-\frac{1}{\rho_0\omega^2}\left(1+\frac{2k_z v_0(r)}{\omega}\right)\frac{\mathrm{d}v_0(r)}{\mathrm{d}r}\frac{\mathrm{d}\varphi_p(r)}{\mathrm{d}r}\right)=0, \tag{19}$$

where T_0 are calculated by equation(9). Moreover, the fluid velocity in equation (15) is

$$\begin{aligned}
v_r' &= \frac{\mathrm{j}}{\rho_0\omega}\left(1+\frac{k_z v_0(r)}{\omega}\right)\frac{\mathrm{d}\varphi_p(r)}{\mathrm{d}r}\exp\left(\mathrm{j}(\omega t-k_z z)\right),\\
v_z' &= \left(\frac{k_z}{\rho_0\omega}\left(1+\frac{k_z v_0(r)}{\omega}\right)\varphi_p(r)\right.\\
&\quad\left.-\frac{1}{\rho_0\omega^2}\left(1+\frac{2k_z v_0(r)}{\omega}\right)\frac{\mathrm{d}v_0(r)}{\mathrm{d}r}\frac{\mathrm{d}\varphi_p(r)}{\mathrm{d}r}\right)\\
&\quad\cdot\exp\left(\mathrm{j}(\omega t-k_z z)\right).
\end{aligned} \tag{20}$$

From equation (18), wave propagation in inviscid fluid is governed by two-order differential equations with unknown functions φ_p, φ_T, and axial wave number k_z. In the end, the rigid wall boundary conditions are zero acoustic velocity in radial direction at the wall defined by

$$v_r'\big|_{r=R}=0 \quad\Rightarrow\quad \frac{\mathrm{d}\varphi_p(r)}{\mathrm{d}r}\Big|_{r=R}=0. \tag{21}$$

2.2. Solution based on Bessel-Fourier theory

From equation (17), it can be verified that functions $\varphi_p(r)$ and $\varphi_T(r)$ can be formulated in the form of zeroth-order Bessel series as shown in Figure 2.

$$\varphi_p(r)=\sum_{n=1}^{\infty}C_n^p J_0(\lambda_n r),\quad \varphi_T(r)=\sum_{n=1}^{\infty}C_n^t J_0(\lambda_n r), \tag{22}$$

where the coefficients C_n^p and C_n^T are determined by

$$\begin{aligned}
C_n^p &= \frac{2}{R^2J_0^2(\lambda_n R)}\int_0^R \varphi_p(r)J_0(\lambda_n r)\,r\,\mathrm{d}r,\\
C_n^T &= \frac{2}{R^2J_0^2(\lambda_n R)}\int_0^R \varphi_T(r)J_0(\lambda_n r)\,r\,\mathrm{d}r,
\end{aligned} \tag{23}$$

and λ_n is the root of boundary condition as shown in equation (21)

$$J_1(\lambda_n R)=0,\quad n=1,2,\ldots, \tag{24}$$

$J_0(\lambda_n R)$ $(n=1,2,\ldots)$ is the orthogonal set of Bessel functions which is complete in Lebesgue Space [40, 41, 42] and has the following property:

$$\int_0^R J_0(\lambda_m r)\,J_0^2(\lambda_n r)r\,\mathrm{d}r=\begin{cases}0 & m\neq n,\\ \dfrac{R^2}{2}J_0^2(\lambda_n R), & m=n.\end{cases} \tag{25}$$

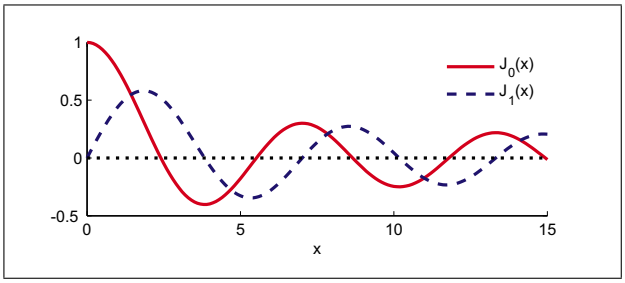

Figure 2. Bessel Functions $J_0(x)$ and $J_1(x)$.

Substituting equation (22) into equation (18) gives

$$\sum_{n=1}^{\infty}C_n^p\left\{\left[\frac{\omega^2-2k_z\omega v_0(r)}{c^2(T_0)}-k_z^2-\lambda_n^2\right]J_0(\lambda_n r)\right.$$
$$\left.-\frac{2k_z\lambda_n}{\omega}\left(1+\frac{k_z v_0(r)}{\omega}\right)\frac{\mathrm{d}v_0(r)}{\mathrm{d}r}J_1(\lambda_n r)\right\}=0,$$
$$\sum_{n=1}^{\infty}C_n^T\left[-\kappa\lambda_n^2+\mathrm{j}\left(k_z v_0(r)-\omega\right)-\kappa k_z^2\right]J_0(\lambda_n r)=$$
$$\sum_{n=1}^{\infty}-C_n^p\left\{\frac{\mathrm{j}\lambda_n}{\rho_0\omega}\left(1+\frac{k_z v_0(r)}{\omega}\right)\frac{\partial T_0}{\partial r}J_1(\lambda_n r)\right. \tag{26}$$
$$-\frac{\partial T_0}{\partial r}\left[\frac{k_z}{\rho_0\omega}\left(1+\frac{k_z v_0(r)}{\omega}\right)J_0(\lambda_n r)\right.$$
$$\left.\left.+\frac{\lambda_n}{\rho_0\omega^2}\left(1+\frac{2k_z v_0(r)}{\omega}\right)\frac{\mathrm{d}v_0(r)}{\mathrm{d}r}J_1(\lambda_n r)\right]\right\}.$$

Moving terms including $v_0(r)$, $\mathrm{d}v_0(r)/\mathrm{d}r$, $c_0^2(T_0)$, $\partial T_0/\partial r$, and $\partial T_0/\partial z$ to the right side and the others to the left of each equation yield

$$\begin{aligned}
&\sum_{n=1}^{\infty}\left(k_z^2+\lambda_n^2\right)J_0(\lambda_n r)C_n^p=\sum_{n=1}^{\infty}H_n^pC_n^p,\\
&\sum_{n=1}^{\infty}-\left(\kappa\lambda_n^2+\mathrm{j}\omega+\kappa k_z^2\right)J_0(\lambda_n r)C_n^T=\\
&\quad\sum_{n=1}^{\infty}I_n^pC_n^p+I_nTC_n^T,
\end{aligned} \tag{27}$$

with

$$\begin{aligned}
H_n^p &= \frac{\omega^2-2k_z\omega v_0(r)}{c^2(T_0)}J_0(\lambda_n r)\\
&\quad-\frac{2k_z\lambda_n}{\omega}\left(1+\frac{k_z v_0(r)}{\omega}\right)\frac{\mathrm{d}v_0(r)}{\mathrm{d}r}J_1(\lambda_n r),\\
I_n^p &= \frac{k_z}{\rho_0\omega}\left(1+\frac{k_z v_0(r)}{\omega}\right)\frac{\partial T_0}{\partial z}J_0(\lambda_n r)\\
&\quad+\left(\frac{1}{\omega}\left(1+\frac{2k_z v_0(r)}{\omega}\right)\frac{\mathrm{d}v_0(r)}{\mathrm{d}r}\frac{\partial T_0}{\partial z}\right.\\
&\quad\left.-\mathrm{j}\left(1+\frac{k_z v_0(r)}{\omega}\right)\frac{\partial T_0}{\partial z}\right)\frac{\lambda_n}{\rho_0\omega}J_1(\lambda_n r),\\
I_n^T &= -\mathrm{j}k_z v_0(r)J_0(\lambda_n r),
\end{aligned} \tag{28}$$

multiplying $J_0(\lambda_m r)r$ to equation (27) and then integrating over the range of $r \in [0, R]$ give

$$\begin{aligned}\left(k_z^2+\lambda_n^2\right)C_m^p &= \frac{2}{R^2J_0^2(\lambda_m R)}\sum_{n=1}^{\infty}\int_0^R C_n^p H_n^p J_0(\lambda_m r)\, r\,\mathrm{d}r,\\ -\left(\mathrm{j}\omega+\kappa\lambda_m^2+\kappa k_z^2\right)C_m^T &= \\ \frac{2}{R^2J_0^2(\lambda_m R)}\sum_{n=1}^{\infty}\int_0^R &\left(I_n^p C_n^p + I_n^T C_n^T\right)J_0(\lambda_m r)\, r\,\mathrm{d}r,\end{aligned} \tag{29}$$

using Bessel sequence, the second-order differential equations in (18) are transformed to algebraic equations where the variables to be solved are the coefficients (C_m^p and C_m^T) of the Bessel sequence and the axial wave number k_z.

2.3. General calculation procedure

Obviously, given specific mean flow $v_0(r)$, angular frequency ω, pipeline radius R, density ρ_0, and the orthogonal Bessel functions $J_0(\lambda_n r)$ with their corresponding eigenvalues λ_n, $n = 1, 2, \ldots, N$ being the roots of the first-order Bessel function $J_1(\lambda_n R) = 0$ from boundary condition defined by equation (24). Expanding equation (29) gives a set of algebraic equations with the unknown parameters C_n^p and C_n^T as well as the axial wave number k_z. A careful investigation reveals that the number of unknown variables is $2N + 1$ while the number of algebraic equations expanded from equation (29) is $2N$, leading to the conclusion that the problem can't been solved until another condition is given. The reason is that the velocity potential Φ and acoustic pressure p' are determined by the energy from the acoustic source which is not given by the present boundary condition.

While the specific coefficients C_n^p and C_n^Φ can't be solved from equation (29) at the present boundary condition (24), the axial wave number k_z can be obtained. It is clearly that taking the coefficients C_n^p and C_n^Φ as unknown variables and expressing them in vector form with $\boldsymbol{X} = [C_1^p \ldots C_N^p \quad C_1^\Phi \ldots C_N^\Phi]$, expanding equation (29) gives a set of linear equations expressed in the matrix form

$$\boldsymbol{G}(k_z)\boldsymbol{X} = 0, \tag{30}$$

where the determinant $\boldsymbol{G}(k_z)$ is a matrix of a dimension $2N \times 2N$, and has the following form (partly shown)

$$\boldsymbol{G}(k_z) = \begin{bmatrix} (k_z^2+\lambda_1^2)+A_1^1 & \cdots & A_1^N & & \\ \vdots & \vdots & \vdots & & \\ A_N^1 & \cdots & (k_z^2+\lambda_N^2)+A_N^N & \cdots & \\ B_1^1 & \cdots & B_1^N & & \\ \vdots & \vdots & \vdots & & \\ B_N^1 & \cdots & B_N^N & & \end{bmatrix}$$
$$\begin{bmatrix} 0 & \cdots \\ \vdots & \vdots \\ 0 & \cdots \\ -(\mathrm{j}\omega+\kappa\lambda_1^2+\kappa k_z^2)+D_1^1 & \cdots \\ \vdots & \vdots \\ D_N^1 & \cdots \end{bmatrix} \tag{31}$$

with

$$\begin{aligned} A_m^n &= -\frac{2}{R^2J_0^2(\lambda_m R)}\int_0^R H_n^p J_0(\lambda_m r)\, r\,\mathrm{d}r,\\ B_m^n &= -\frac{2}{R^2J_0^2(\lambda_m R)}\int_0^R I_n^p J_0(\lambda_m r)\, r\,\mathrm{d}r,\\ D_m^n &= -\frac{2}{R^2J_0^2(\lambda_m R)}\int_0^R I_n^T J_0(\lambda_m r)\, r\,\mathrm{d}r. \end{aligned}$$

From equation (31), it shows that the coefficients do not vanish at the same time, leading to the condition of $\boldsymbol{X} \neq 0$. Then the condition of non-trivial solution existence for homogeneous linear equations in (31) is that the determinant of $G(k_z)$ vanishes, leading to a nonlinear function of the axial wave number k_z expressed by

$$\det\left(\boldsymbol{G}(k_z)\right) = 0, \tag{32}$$

the above function is nonlinear and can be solved by various numerical methods in the literature.

3. Numeric Calculation and Discussion

In this section, wave propagation (phase velocity, acoustic and temperature distribution along the cross-section) for heating pipeline is discussed and parametric analysis of measurement performance of transit-time flow meter is given for laminar and turbulent flow based on the work of Willatzen [1, 2]. As shown in [2], the steady temperature for heating pipe in equation (9) is governed by

$$\begin{aligned} T_0 &= \overline{T}_0 + \zeta z + g(r),\\ \frac{1}{r}\frac{\mathrm{d}}{\mathrm{d}r}\left(r\frac{\mathrm{d}g(r)}{\mathrm{d}r}\right) &= \frac{\zeta v_0(r)}{\kappa}, \end{aligned} \tag{33}$$

where $\overline{T}_0$ is the temperature near the pipeline, ζ is the temperature axial gradient, $g(r)$ is a function of the radial coordinate. In the numerical calculation, sound isothermal velocity [48] $c(T_0)$ can be expressed by

$$c(T_0) \approx 1449.2 + 4.6T_0 - 0.055T_0^2 + 0.00029T_0^3. \tag{34}$$

In the end, the deviation [30, 31, 36, 47, 49] of measurement E_n is used as a quality measurement for transit-time flow meter,

$$E_n = \frac{\Delta t_n - \Delta t_0}{\Delta t_0}, \tag{35}$$

where Δt_0 is the transit time difference of the fundamental mode expressed by

$$\Delta t_0 = \frac{2L\overline{v}}{c_0^2(T_0)}, \tag{36}$$

and Δt_n is the transit time difference of the nth order mode

$$\Delta t_n = \frac{\Delta\phi}{\omega} = \frac{L}{\omega}\left((k_z^n)^- - (k_z^n)^+\right), \tag{37}$$

L is the pipeline length, and ω is the angular frequency.

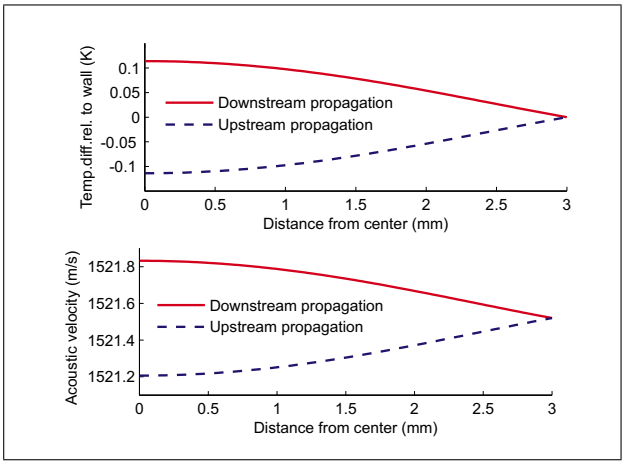

Figure 3. Temperature (upper) and acoustic velocity (lower) variations induced by laminar flow profile $U = 0.1$ m/s for downstream and upstream propagation in cylindrical waveguide with $R = 3$ mm and $\zeta = -0.05$ K/m. Data for water at $\overline{T}_0 = 20$°C is used.

3.1. Laminar flow profile

3.1.1. Wave propagation analysis

Based on [43, 44], laminar flow profile can be described by Poisson's equation

$$v_0(r) = 2U\left(1 - \frac{r^2}{R^2}\right), \tag{38}$$

where U is the average amplitude value of the velocity. In this section, Parameters are $U = 0.1$ m/s, $R = 3$ mm, $\zeta = -0.05$ K/m, $Pr = \nu/\kappa = 6.75$, and $\nu = 10^{-6}$ m^2/s where ν and Pr are kinematic viscosity and Prandtl number. Figure 3 shows the temperature difference relative to wall temperature ($g(r)$ in equation 33) and acoustic velocity in equation (34) along the axial coordinate in downstream and upstream propagation when the temperature of fluid $\overline{T}_0$ is 20 °C.

In Figure 3, temperature increases along the axial direction in downstream propagation and decreases in upstream propagation. As a result, acoustic velocity falls down in downstream flow and grows up in upstream flow. Under the same situation, variations of phase velocity ($c_p = 2\pi f/k_z$) of the first four patterns in downstream and upstream propagation with mean fluid flow $U = 0.1$ m/s are shown in Figure 4 for wave frequency $f = 2$ MHz and $f = 3$ MHz.

From Figure 4, it is evident that for every pattern, phase velocity in downstream propagation grows up as temperature gradient ζ in axial direction decreases while phase velocity in upstream propagation declines. The difference of phase velocity between downstream and upstream propagation turns out to be larger in the presence of temperature gradient comparing with the difference in the absence of temperature gradient, leading to the conclusion that transit-time difference of wave propagation between upstream and downstream flow builds up in heating pipeline as shown in equation (37), and thus it becomes easier to

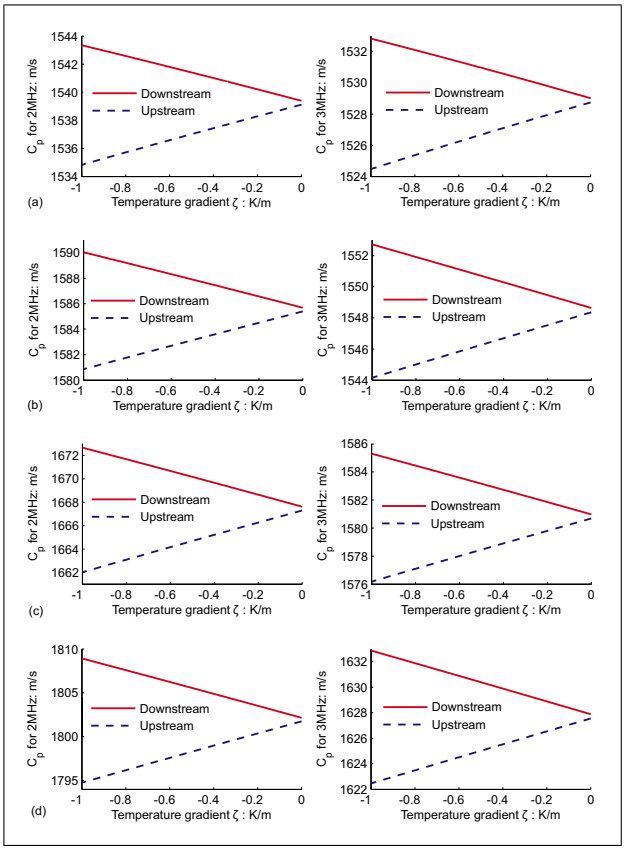

Figure 4. Phase velocity of the first four patterns in downstream and upstream wave propagation of frequency $f = 2$ MHz and $f = 3$ MHz with radius $R = 3$ mm. Data for water at $\overline{T}_0 = 20$°C is used and a mean flow equals $U = 0.1$ m/s.

be measured than that without temperature gradient. Furthermore, it is obvious that phase velocity of each pattern is smaller in higher frequency than in lower frequency.

Using the same parameters, Figures 5 and 6 show the acoustic pressure distribution $\varphi_p(r)$ and corresponding temperature amplitude distribution $\varphi_T(r)$ (in equation (22) with $f = 2$ MHz) of the first four patterns relatively in pipeline $R = 3$ mm and flow velocity $U = 0.1$ m/s.

From Figure 6, acoustics pressure is different between patterns where acoustic pressure distribution of higher pattern is more complicated than that of lower pattern. Pressure in the center of the pipeline cross section is the largest around the whole cross section. There is not explicit difference of pressure distributions between downstream and upstream propagation. The corresponding temperature distribution is more complex than pressure distribution. A common phenomenon is that higher pattern increases the complexity of pressure and temperature distributions in the cross section and propagation direction (upstream and downstream propagation) doesn't impose significant contributions to pressure and temperature distributions.

3.1.2. Analysis of measurement performance

In this section, parametric analysis of measurement performance is discussed to give a detail understanding of

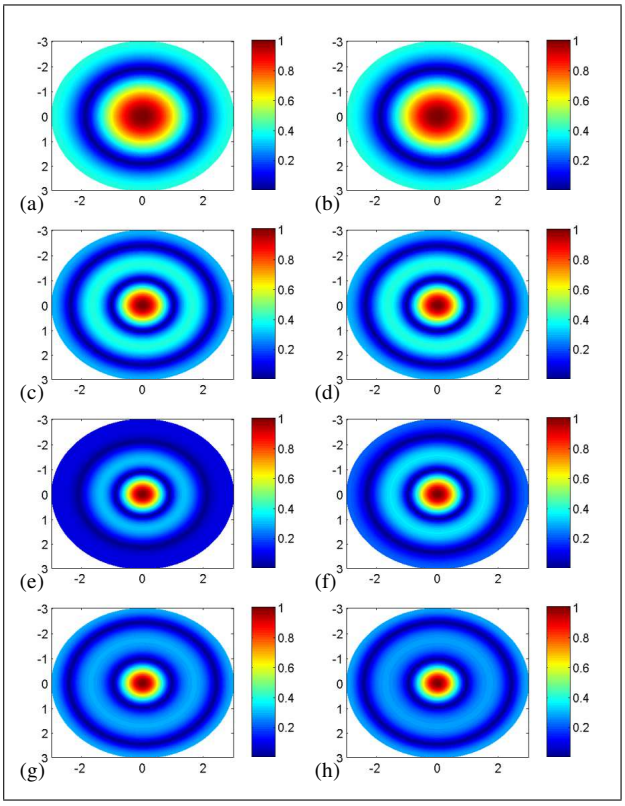

Figure 5. Normalized pressure distribution of the first four patterns in fluid flow $U = 0.1$ m/s. Other parameters used are $R = 3$ mm, $\zeta = -0.05$ K/m and $\overline{T}_0 = 20$°C for water. a: first mode in downstream propagation; b: first mode in upstream propagation; c: second mode in downstream propagation; d: second mode in upstream propagation; e: third mode in downstream propagation; f: third mode in upstream propagation; g: fourth mode in downstream propagation; h: fourth mode in upstream propagation.

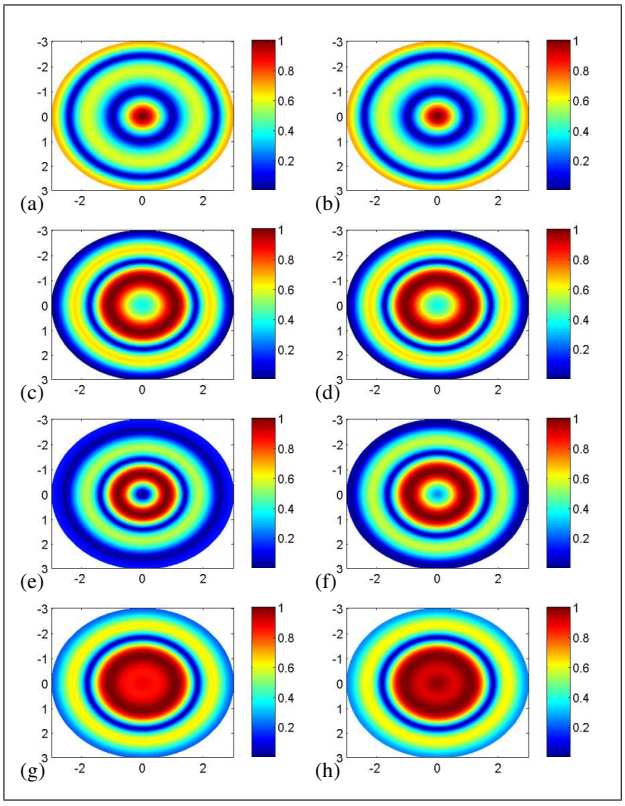

Figure 6. Normalized temperature distribution of the first four patterns in fluid flow $U = 0.1$ m/s. Other parameters are $R = 3$ mm, $\zeta = -0.05$ K/m and $\overline{T}_0 = 20$°C for water. a: first pattern for downstream propagation; b: first pattern for upstream propagation; c: second pattern for downstream propagation; d: second pattern for upstream propagation; e: third pattern for downstream propagation; f: third pattern for upstream propagation; g: fourth pattern for downstream propagation; h: fourth pattern for upstream propagation.

performance of ultrasonic transit-time flow meter in laminar flow. In this section, the velocity of fluid flow is in the range of $U = 0.001$ m/s–0.1 m/s and $\overline{T}_0 = 20$°C. Figure 7 shows the measurement deviations in equation (35) of the first four patterns with frequency $f = 2$ MHz and $f = 3$ MHz for $R = 3$ mm in the absence of temperature gradient $\zeta = 0$ K/m and Figure 8 reveals the corresponding results in the case of $R = 9$ mm, Figures 9 and 10 display the results of $\zeta = -0.005$ K/m.

From Figures 7–10, the deviations E_n of measurement for smaller mean flow vibrate more seriously comparing with larger mean flow while measurement deviances for higher pattern are larger than those for lower pattern. Moreover, vibrations of E_n with higher frequency are more serious than lower frequency. As a result, reducing the ultrasound frequency f may be a possible way to diminish the influence of temperature gradient on flow meter performance which is consistent with the work of Willatzen [1, 2], however the improvement is not significant. Moreover, deviations of measurement are smaller with pipeline radius $R = 0.003$ m than those with radius $R = 0.009$ m, suggesting that using small-diameter pipeline is a possible way to reduce the effect of temperature gradient. However, it should be noted that the measurement performance is worse as the temperature gradient in the axial direction becomes bigger comparing with deviations of measurement between $\zeta = 0$ K/m and $\zeta = -0.005$ K/m.

3.2. Turbulent flow profile

3.2.1. Wave propagation analysis

In this section, wave propagation in turbulent flow is addressed while the flow profile can be expressed by [30, 31, 36, 47, 49, 50]

$$v_0(r) = \tau U + (1-\tau)2U\left(1 - \frac{r^2}{R^2}\right), \tag{39}$$

where

$$\tau = 1 - \frac{1}{1 + (\mathrm{Re}/\mathrm{Re}_0)^{\epsilon}}, \quad \mathrm{Re} = 2UR/\nu, \tag{40}$$

and Re_0 is the Reynolds number locating the transition region between the laminar and turbulent flow regime and the exponent $\epsilon = 4$ is chosen in the present work. Figure 11 shows the phase velocity of different patterns in downstream propagation as functions of axial temperature

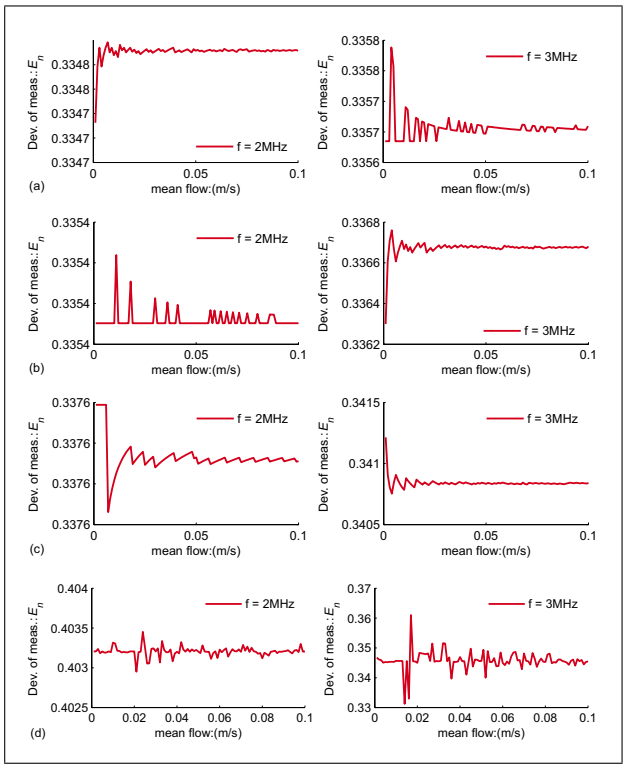

Figure 7. Measurement of the first four patterns for frequency $f = 2\,\text{MHz}$ and $f = 3\,\text{MHz}$ with temperature gradient $\zeta = 0\,\text{K/m}$. Top to down: the first, second, third, fourth pattern. Calculations correspond to pipeline radius $R = 3\,\text{mm}$.

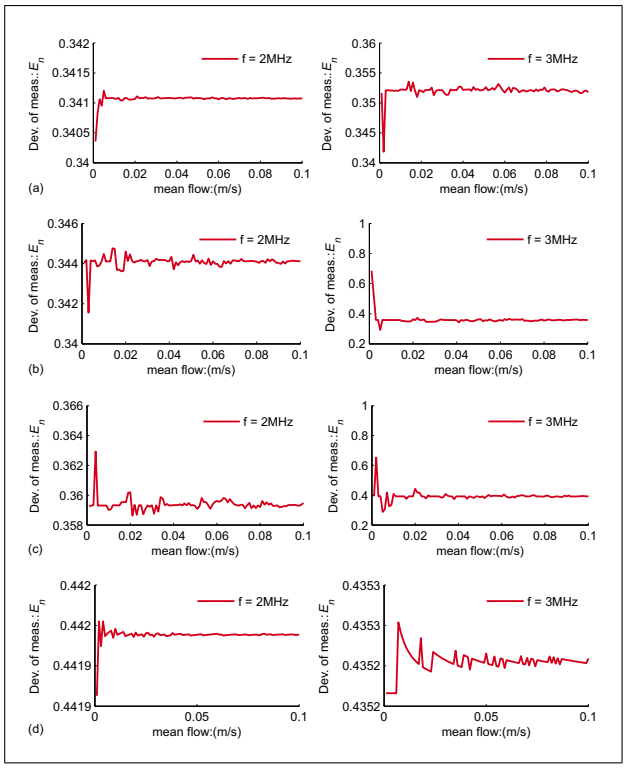

Figure 8. Measurement E_n of the first four patterns for frequency $f = 2\,\text{MHz}$ and $f = 3\,\text{MHz}$ with temperature gradient $\zeta = 0\,\text{K/m}$. Top to down: the first, second, third, fourth pattern. Calculations correspond to pipeline radius $R = 3\,\text{mm}$.

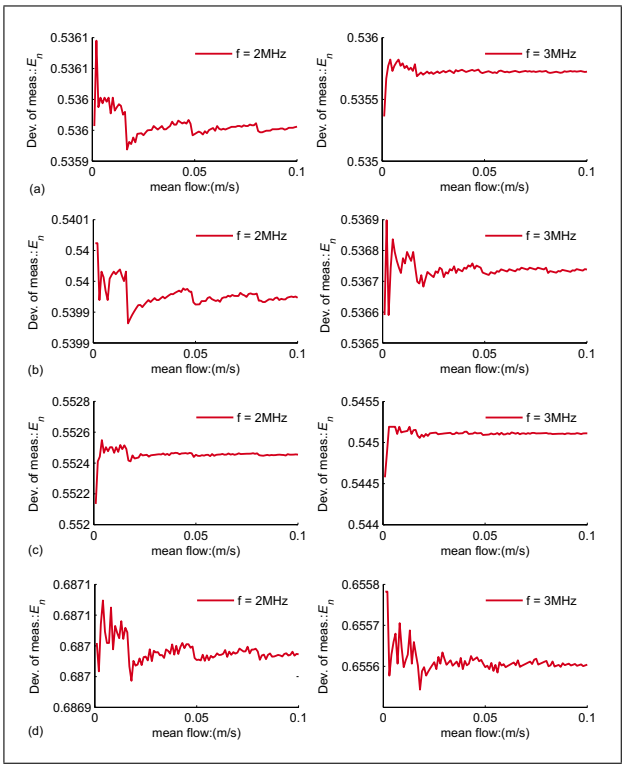

Figure 9. Measurement E_n of the first four patterns for frequency $f = 2\,\text{MHz}$ and $f = 3\,\text{MHz}$ with temperature gradient $\zeta = -0.005\,\text{K/m}$. Top to down: the first, second, third, fourth pattern. Calculations correspond to pipeline radius $R = 3\,\text{mm}$.

gradient for frequency $f = 1\,\text{MHz}$, $f = 2\,\text{MHz}$, and $f = 5\,\text{MHz}$. Parameters used are $R = 9\,\text{mm}$, $Pr = \nu/\kappa = 6.75$, $\nu = 10^{-6}\,\text{m}^2/\text{s}$ $\zeta = -0.05\,\text{K/m}$, $U = 15\,\text{m/s}$, and $\overline{T}_0 = 20°\text{C}$.

Comparing with Figure 4, it is clear that change rates of phase velocity are more complicated in turbulent flow than in laminar flow while phase velocity of wave propagation with lower frequency is more sensitive to axial temperature gradient. Moreover, Figures 12 and 13 show the corresponding acoustic pressure $\varphi_p(r)$ and temperature distribution $\varphi_T(r)$ (equation 22) of the first four patterns in downstream propagation for $f = 2\,\text{MHz}$.

Comparing with acoustics pressure distribution in laminar flow profile as shown in Figure 5, pressure distribution for each wave pattern in turbulent flow is significantly different from that in laminar flow as displayed in Figure 12. This indicates that pressure distribution is sensitive to fluid flow profile. However, as shown in Figure 5, pressure distribution in downstream and upstream propagation is mostly identical. The results hold in the temperature distribution as shown in Figure 13.

3.2.2. Analysis of measurement performance

In this section, parametric analysis of measurement performance is discussed to give a detail understanding of performance of ultrasonic transit-time flow meter in laminar flow. In this section, the velocity of fluid flow is in the range of $U = 0.1\,\text{m/s}$–$15\,\text{m/s}$ and $\overline{T}_0 = 20°\text{C}$. As shown

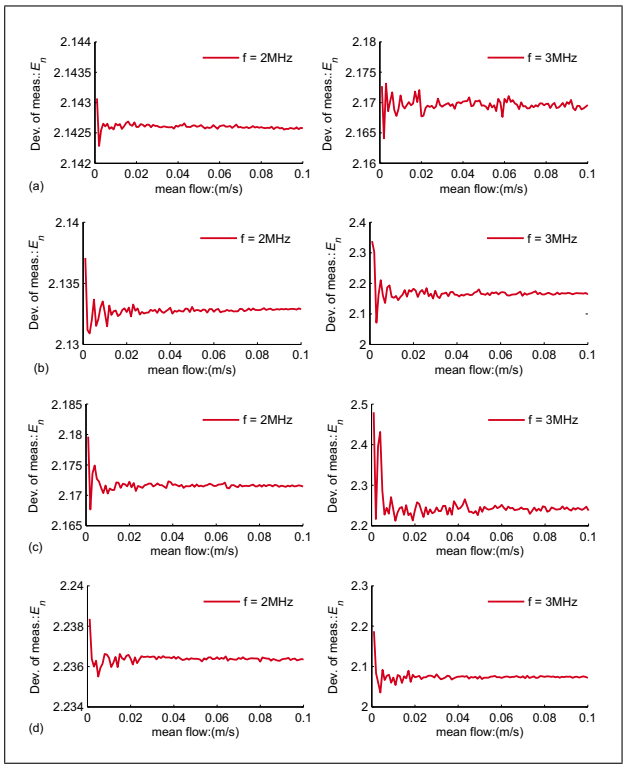

Figure 10. Measurement E_n of the first four patterns for frequency $f = 2\,\text{MHz}$ and $f = 3\,\text{MHz}$ with temperature gradient $\zeta = -0.005\,\text{K/m}$. Top to down: the first, second, third, fourth pattern. Calculations correspond to pipeline radius $R = 9\,\text{mm}$.

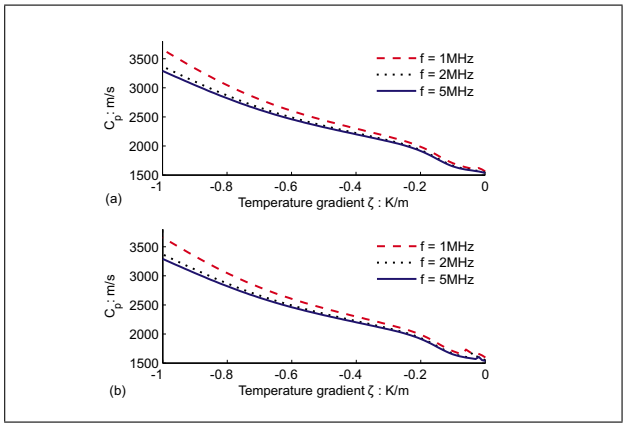

Figure 11. Phase velocity of patterns (the second and third pattern) in turbulent flow with $R = 9\,\text{mm}$ for frequency $f = 2\,\text{MHz}$ (dashed line), $f = 3\,\text{MHz}$ (dotted line) and $f = 5\,\text{MHz}$ (solid line).

in laminar flow, the measurement performance of transit-time flow meter is better in smaller diameter pipeline, this section just addresses flow meter with pipeline radii $R = 3\,\text{mm}$. Figure 14 shows the deviations E_n of measurement in the absence of temperature axial gradient, $\zeta = 0\,\text{K/m}$ and Figure 15 illustrates measurement performance for $\zeta = -0.005\,\text{K/m}$.

Obviously, in turbulent flow without axial temperature gradient $\zeta = 0\,\text{K/m}$, deviations of measurement for all waveguide patterns converge to zero as mean flow velocity

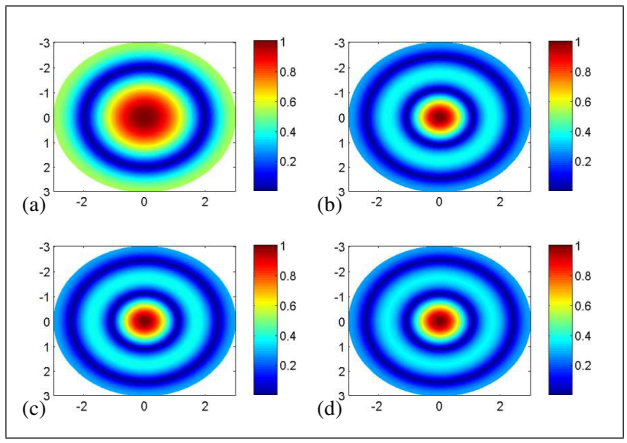

Figure 12. Normalized pressure distribution of the first four patterns in downstream propagation with flow $U = 15\,\text{m/s}$. Other parameters are $R = 3\,\text{mm}$, $\zeta = -0.05\,\text{K/m}$ and $\overline{T}_0 = 20°\text{C}$ for water. a: first mode; b: second mode; c: third mode; d: fourth mode.

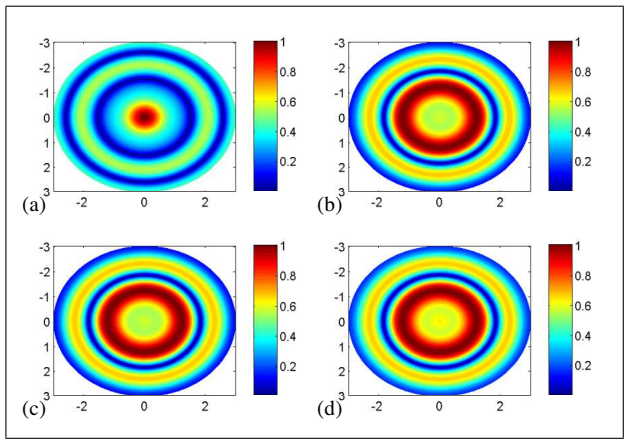

Figure 13. Normalized temperature distribution of the first four patterns in downstream propagation with flow $U = 15\,\text{m/s}$. Other parameters are $R = 3\,\text{mm}$, $\zeta = -0.05\,\text{K/m}$ and $\overline{T}_0 = 20°\text{C}$ for water. a: first mode; b: second mode; c: third mode; d: fourth mode.

builds up for each frequency $f = 2\,\text{MHz}$ and $f = 3\,\text{MHz}$ as shown in Figure 14 while deviations of measurement remain high values in laminar flow as shown in Figures 7 and 8. On the other hand, in the presence of temperature gradient, deviations of measurement for every pattern in turbulent flow increase and converge to constant values as shown in Figure 15. It should be noticed that deviation of measurement with higher frequency performs better than that with lower frequency.

4. Conclusion

Thermal-mechanical wave propagation in inviscid non-uniform flow confined by heating cylindrical pipeline is addressed which turns out to be two second-order differential equations, and a general solution based on the zeroth-order Bessel series, which are orthogonal and complete in Lebesgue Space $\mathcal{L}_r^2(0, R)$ in equation (22), is firstly pro-

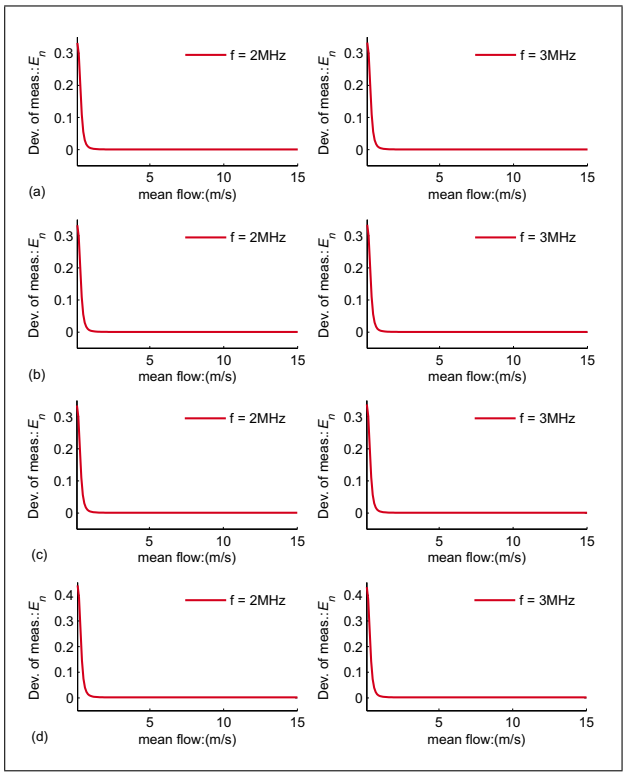

Figure 14. Measurement of the first four patterns for frequency $f = 2\,\mathrm{MHz}$ and $f = 3\,\mathrm{MHz}$ with temperature gradient $\zeta = 0\,\mathrm{K/m}$. Top to down: the first, second, third, fourth pattern. Calculations correspond to pipeline radius $R = 3\,\mathrm{mm}$.

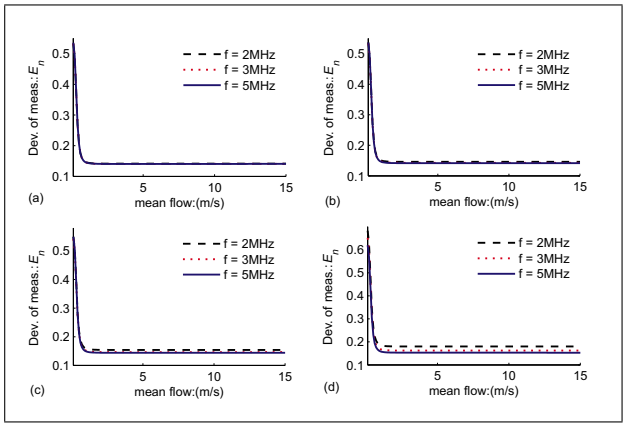

Figure 15. Measurement of the first four patterns for frequency $f = 2\,\mathrm{MHz}$, $f = 3\,\mathrm{MHz}$ and $f = 5\,\mathrm{MHz}$ with temperature gradient $\zeta = -0.005\,\mathrm{K/m}$. Top to down: the first, second, third, fourth pattern. Calculations correspond to pipeline radius.

posed in the literature. Such method transforms the proposed two second-order differential equations expressed in equation (19) to a set of algebraic equations expressed in equation (29) which can be resolved using non-trivial solution of linear algebraic equations as shown in equation (32). Based on the established solution, acoustic velocity, acoustic pressure and temperature distribution in the pipeline circular cross section are calculated and analyzed for both laminar and turbulent flow profile in the presence of axial temperature gradient. Moreover, measurement performance of ultrasonic transit-time flow meter is analyzed for laminar and turbulent flow profile considering different pipeline radii, frequencies and axial temperature gradients. Results show that temperature gradient imposes remarkable influence on the measurement performance while reducing pipeline radii and decreasing frequency may be possible methods to circumvent influence of axial temperature gradient for laminar flow. It should be pointed that results of measurement performance in laminar flow in present paper match well with contributions by Willatzen [1, 2]. However, decreasing frequency leads to lower quality of measurement accuracy in turbulent flow as shown in Figure 15.

Acknowledgement

The work described in this paper was funded by the National Natural Science Foundation of China (No. 50975280 and No. 51205403). This funding is gratefully acknowledged by the authors.

References

[1] M. Willatzen: Ultrasonic flowmeters: temperature gradients and transducer geometry effects. Ultrasonics **41** (2003) 105–114.

[2] M. Willatzen: Temperaure gradients and flow-meter performance. Ultrasonics **39** (2001) 383–389.

[3] I. Gabrielaitiene, B. Bøhm, B. Sunden: Evaluation of approaches for modeling temperature wave propagation in district heating pipelines. Heat Transfer Eng. **29** (2008) 45–56.

[4] A. R. Guilbert, M. Law, M. L. Sanderson: A novel ultrasonic/thermal clamp-on flowmeter for low liquid flowrates in small diameter pipes. Ultrasonics **34** (1996) 435–439.

[5] D. C. Pridmore-Brown: Sound propagation in a fluid flowing through an attenuating duct. J. Fluid Mech. **4** (1958) 393–406.

[6] P. Mungur, H. E. Plumblee: Propagation and attenuation of sound in a soft walled annular duct containing a sheared flow. NASA Report, SP-207, 1969.

[7] N. K. Agarwal, M. K. Bull: Acoustic wave propagation in a pipe with fully developed turbulent flow. J. Sound Vib. **132** (1989) 275–298.

[8] W. Eversman: Effect of boundary layer on the transmission and attenuation of sound in an acoustically treated circular duct. J. Acoust. Soc. Am. **49** (1970) 1372–1380.

[9] W. Eversman: The effect of mach number on the tuning of an acoustic lining in a flow duct. J. Acoust. Soc. Am. **48** (1969) 425–428.

[10] J. F. Unruh, W. Eversman: The utility of the galerkin method for the acoustic transmission in an attenuation duct. J. Sound Vib. **23** (1972) 187–197.

[11] S.-H. Ko: Theoretical prediction of sound attenuation in acoustically lined annular ducts in the presence of uniform flow and shear flow. J. Acoust. Soc. Am. **54** (1973) 1592–1606.

[12] S.-H. Ko: New approach to the solution of eigenvalue problems in circular flow ducts (a Taylor series method). J. Acoust. Soc. Am. **70** (1981) 205–212.

[13] A. H. Nayfeh, J. E. Kaiser, B. S. Shake: A wave-envelope analysis of sound propagation in nonuniform circular ducts

with compressible mean flows. NASA Report, CR-3109, 1979.

[14] W. R. Watson: A finite element simulation of sound attenuation in a finite duct with a peripherally variable liner. NASA Report, TM-74080, 1977.

[15] R. J. Astley, W. Eversman: A finite element method for transmission in non-uniform ducts without flow: comparison with the method of weighted residuals. J. Sound Vib. **57** (1978) 367–388.

[16] R. J. Astely, W. Eversman: A finite element formulation of the eigenvalue problem in lined ducts with flow. J. Sound Vib. **65** (1979) 61–74.

[17] K. A. Kousen: Eigenmodes of ducted flows with radially-dependent axial and swirl velocity components. NASA Report, CR-1999-208881, 1999.

[18] C. Bailly, D. Juve: Numerical solution of acoustic propagation problems using linearized Euler equations. AIAA J. **38** (2000) 22–29.

[19] H. Ju, K.-Y. Fung: A time-domain method for duct acoustics. J. Sound Vib. **237** (2000) 667–681.

[20] W. Eversman, E. L. Cook, R. J. Beckemeyer: A method of weighted residuals for the investigation of sound transmission in non-uniform ducts without flow. J. Sound Vib. **38** (1975) 105–123.

[21] W. Eversman: Intial values for the integration scheme to compute the eigenvalues for propagation in ducts. J. Sound Vib. **50** (1977) 159–162.

[22] P. T. Vo, W. Eversman: A method of weighted residuals with trigonometric basis functions for sound transmission in circular ducts. J. Sound Vib. **56** (1978) 243–250.

[23] W. Eversman, R. J. Astley: Acoustic transmission in non-uniform ducts with mean flow. Part I: The method of weighted residuals. J. Sound Vib. **74** (1981) 89–101.

[24] R. Mani: Sound propagation in parallel sheared flows in ducts: the mode estimation problem. Proc. R. Soc. Lond. A **371** (1980) 393–412.

[25] G. R. Gogate, M. L. Munjal: Sound propagation in ducts with bulk reacting lining in the presence of laminar mean flow. J. Acoust. Soc. Am. **99** (1996) 1779–1782.

[26] G. R. Gogate, M. L. Munjal: Analytical solution of the laminar mean flow wave equation in a lined or unlined two-dimensional rectangular duct. J. Acoust. Soc. Am. **92** (1992) 2915–2923.

[27] G. R. Gogate, M. L. Munjal: Analytical solution of sound propagation in lined or unlined circular ducts with laminar mean flow. J. Sound Vib. **160** (1993) 465–484.

[28] R. Boucheron, H. Bailliet, J.-C. Valiere: Analytical solution of multimodal acoustic propagation in circular ducts with laminar mean flow profile. J. Sound Vib. **292** (2006) 504–518.

[29] H. Lechner: Ultrasonic flow metering based on transit time differentials which are insensitive to flow profile. J. Acoust. Soc. Am. **74** (1983) 955–959.

[30] M. Willatzen: Comments on "Ultrasonic flow metering based on transit time differentials which are insensitive to flow profile". J. Acoust. Soc. Am. **107** (2000) 1762–1765.

[31] M. Willatzen: Sound propagation in a moving fluid confined by cylindrical walls – a comparison between an exact analysis and the local-plane wave approximation. J. Sound Vib. **247** (2001) 719–729.

[32] W. Eversman, R. J. Beckemeyer: Transmission of sound in ducts with thin shear layers-convergence to the uniform flow case. J. Acoust. Soc. Am. **52** (1972) 216–220.

[33] M. Willatzen: Ultrasonic flow measurement and wall acoustic impedance effects. Ultrasonics **41** (2004) 719–726.

[34] V. Pagneux, B. Froelich: Influence of low mach number shear flow on acoustic propagation in ducts. J. Sound Vib. **246** (2001) 137–155.

[35] B. Robertson: Effect of arbitrary temperature and flow profiles on the speed of sound in a pipe. J. Acoust. Soc. Am. **62** (1977) 813–818.

[36] M. Willatzen: Perturbation theory applied to sound propagation in flowing media confined by a cylindrical waveguide. J. Acoust. Soc. Am. **109** (2001) 102–107.

[37] J. C. Wendoloskia: On the theory of acoustic flow measurement. J. Acoust. Soc. Am. **110** (2001) 724–737.

[38] F. Treyssede, G. Gabard, M. B. Tahar: A mixed finite element method for acoustic wave propagation in moving fluids based on an Eulerian-Lagrangian description. J. Acoust. Soc. Am. **113** (2003) 705–716.

[39] G. Gabard, F. Treyssede, M. B. Tahar: A numerical method for vibro-acoustic problems with sheared mean flows. J. Sound Vib. **272** (2004) 991–1011.

[40] G. Arfken: Mathematical methods for physicists. Academic Press, 1985.

[41] S. Hassani: Mathematical methods: for students of physics and related fields. Springer, 2008.

[42] M. A. Al-Gwaiz: Sturm-Liouville theory and its applications. Springer-Verlag, 2008.

[43] L. D. Landau, E. M. Lifshitz: Fluid mechanics. Linacre House, Jordan Hill, Oxford, 1987.

[44] A. L.Fetter, J. D. Walecka: Theoretical mechanics of particles and continua. McGraw-Hill, 2003.

[45] D. Blokhintzev: The propagation of sound in an inhomogeneous and moving medium I. J. Acoust. Soc. Am. **18** (1946) 322–328.

[46] F. M. White: Viscous fluid flow. McGraw-Hill, 1991.

[47] M. Willatzen: Liquid flows and vibration characteristics of straight-tube cylindrical shells. j. Sound Vib. **260** (2003) 417–429.

[48] L. Wang, K. L. McCarthy, M. J. McCarthy: Effect of temperature gradient on ultrasonic Doppler velocimetry measurement during pipe flow. Food Res. Int. **37** (2004) 633–642.

[49] M. Willatzen: Flow acoustics modelling and implications for ultrasonic flow measurement based on the transit-time method. Ultrasonics **41** (2004) 805–810.

[50] M. Willatzen: Phase shift and attenuation characteristics of acoustic waves in a flowing gas confined by cylindrical walls. J. Sound Vib. **261** (2003) 791–803.